Numerical study of the Marangoni instability resulting in surface tension auto-oscillations: General regularities of the system evolution

N. M. Kovalchuk,[1] V. I. Kovalchuk,[2] and D. Vollhardt[3,*]
[1]*Institute for Problems of Material Science, Kiev, Ukraine*
[2]*Institute of Biocolloid Chemistry, Kiev, Ukraine*
[3]*Max-Planck-Institute of Colloids and Interfaces, 14424 Potsdam/Golm, Germany*
(Received 23 June 2000; published 27 February 2001)

Theoretical studies are performed to explain the mechanism of surface tension auto-oscillations recently found. The Marangoni instability in a system containing a surfactant droplet under the air-water interface is investigated numerically. The simulations, based on the equations of fluid mechanics, take into account convective diffusion and adsorption of the surfactant. The behavior of the system is determined by nonstationary concentration gradients that are nonuniform on the surface as well as in the normal to the surface direction. Initially a slow diffusion dissolution of the drop material takes place. The convective transfer of the surfactant is negligible, the surface tension remains nearly constant and the system parameters change rather slowly during the induction period. With the increase of the concentration gradients the system becomes unstable, resulting in a jump in the convection velocity, surface tension, and adsorption on the surface. The concentration and velocity distributions in the bulk and on the surface are obtained from the numerical solution of the problem. The contributions of different mechanisms of the mass transfer are compared in different stages of the process.

DOI: 10.1103/PhysRevE.63.031604 PACS number(s): 47.20.Dr, 68.03.−g, 47.20.Ma, 68.35.Fx

INTRODUCTION

The presence of temperature or concentration gradients in a liquid system with a free interface can be the reason for instability and formation of various dissipative structures, such as steady convective cells or transverse and longitudinal waves [1]. One of the mechanisms leading to instability is related to the Marangoni effect (i.e., to the action of a surface tension gradient). Experimental evidence of this kind of instability is given, see, e.g., [2–8].

Although the governing equations describing the nonstationary transfer of heat and mass are the same, some distinction can be in boundary conditions, in particular related to the adsorption processes. That is the reason why systems with nonuniform concentration distribution require independent consideration. The theoretical investigation of this problem was started by Sternling and Scriven [9]. They studied the processes at the interface between two semi-infinite liquid phases in the presence of a concentration gradient of the third component in each of the liquids. Using small disturbance analysis they determined the conditions under which instabilities can exist in such a system. The theory was further developed in a number of subsequent works [10–17], which provide a comprehensive basis for the explanation of the experimental results.

Recent experiments show an interesting phenomenon also associated with the surface tension driven instability. It is the development of auto-oscillations of the surface tension when a surfactant droplet is placed in the bulk of water [18]. The auto-oscillations are characterized by an abrupt decrease of the surface tension after a relatively stable phase of system evolution. The impressive feature of this phenomenon is the existence of spontaneous oscillations over a long period of time. As shown in [18], a diethyl phthalate droplet with a diameter of about 3 mm can sustain oscillations for more than 8 h. In our recent experiments with aliphatic alcohols the auto-oscillations were observed for over 72 h [19]. The peculiarity of this effect is that the auto-oscillations are caused by solute transfer from the bulk of the liquid to the air-liquid interface. It is known, however, that usually oscillatory instability reveals itself by mass transfer in the opposite direction [8,15]. New theoretical studies are necessary to explain the mechanism of the surface tension auto-oscillations because recent findings indicate a different origin than those considered earlier.

The behavior of the system with a surfactant droplet under the free liquid surface is determined by a concentration gradient that changes over time and is nonuniform in space both tangential and normal to the surface. It demands a comprehensive theoretical investigation that takes into account nonstationary states of the concentration gradient and the complicated geometry of the system. The qualitative explanation of the phenomenon of surface tension auto-oscillations presented in [18] considers two different stages in the dynamic behavior of the system, a slow stage and a fast stage. At first, during the slow stage, convection is small and almost all of the mass transfer of the surfactant into the system is due to diffusion. Next, during the fast stage, instability arises in the system, convection develops rapidly and accelerates the transfer of surfactant to the surface.

In the present paper we focus our theoretical studies on the mechanism of the surface tension auto-oscillations. The system considered is characterized by a set of nonstationary partial differential equations. The equations cannot be linear-

*Author to whom correspondence should be addressed.

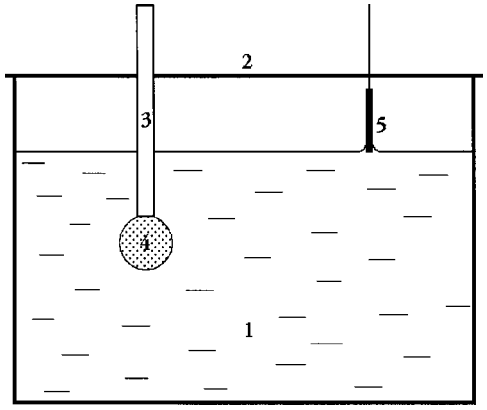

FIG. 1. Measuring cell for the study of auto-oscillations of surface tension. 1, Water; 2, covering plate; 3, capillary; 4, surfactant droplet; 5, Wilhelmy plate.

ized because the variations of all the functions are large and the nonlinear effects play an important role in the mechanism of the auto-oscillations. Therefore direct numerical computations that focus on the simulation of the processes of convective diffusion and adsorption in a system consisting of a semi-infinite liquid layer were chosen as the method to solve the problem.

EXPERIMENTAL SECTION

At first the phenomenon of surface tension auto-oscillations was revealed for diethyl phthalate (DEP) [18]. A schematic representation of the tensiometric setup, including the measuring cell, where the experiments were performed is given in Fig. 1. The experimental procedure used is as follows. A glass vessel was filled with ultra pure water (1) and the water surface was cleaned to prevent contamination. Then the vessel was covered with a glass plate (2); a glass capillary (3) was introduced through an opening in a glass cover and immersed into the water. A platinum Wilhelmy plate (5) was then introduced to measure the surface tension. Finally a surfactant droplet (4) was formed at the tip of the capillary and the measurements were started.

The results described in [18] were obtained by using a thermostated measuring cell at a temperature of 30 °C. New experiments were carried out with DEP and mediate-chain alcohols at the room temperature [19]. One of the experimental curves for DEP at the room temperature is shown in Fig. 2. It is seen that during a certain time interval, denoted as induction period, the surface tension did not change remarkably. The duration of the induction period depends on the immersion depth of the capillary. In the experiment presented the induction time is approximately 12 min for a capillary immersion depth of 6.2 mm. After this induction time surface tension auto-oscillations begin spontaneously. The period of this oscillation is about 14 min, the amplitude is about 1.5–2.5 mN/m. The oscillation has an asymmetric shape with a sharp decrease in surface tension followed by gradual increase.

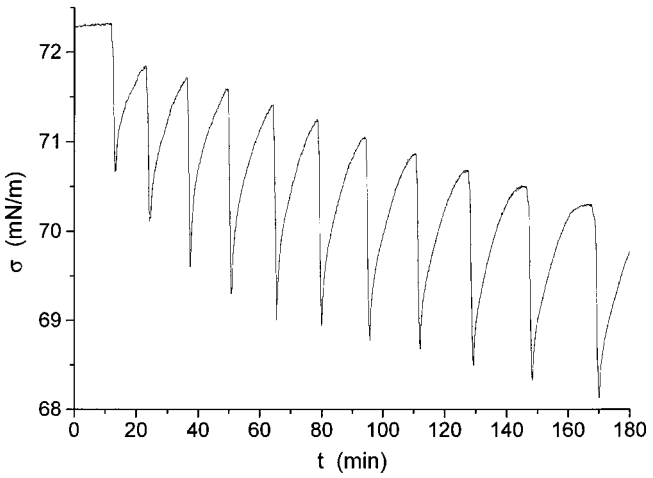

FIG. 2. Experimental data of the auto-oscillations of surface tension [19].

THEORETICAL MODEL

To model the system for the numerical simulation, it is appropriate to consider a semi-infinite liquid volume with a free air-water interface and a spherical surfactant droplet submersed into the liquid (Fig. 3). Although the model had infinite dimensions and neglects the presence of the capillary, the simulation shows that it is subjected to the same regularities as the experimental system shown in Fig. 1. Therefore, the model is appropriate to analyze the details of the mechanism governing the surface tension auto-oscillations.

The dynamic behavior of the system is described by a set of non-steady-state Navier-Stokes equation (1), the continuity equation (2), and the convective diffusion equation (3):

$$\rho \frac{\partial \mathbf{v}}{\partial t} + \rho \mathbf{v} \cdot \nabla \mathbf{v} = -\nabla \mathbf{p} + \mu \Delta \mathbf{v}, \tag{1}$$

$$\nabla \cdot \mathbf{v} = 0, \tag{2}$$

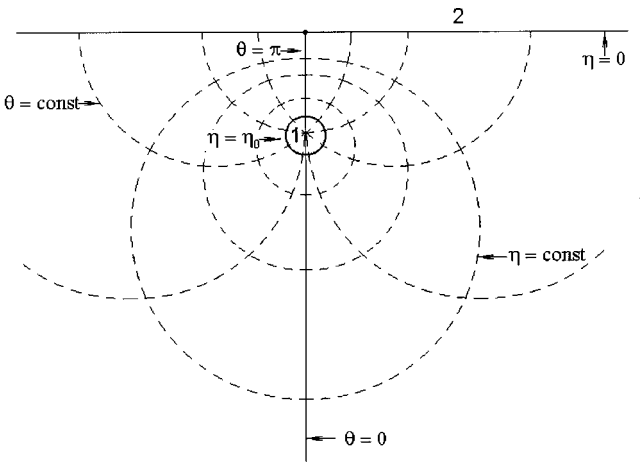

FIG. 3. Application of bipolar coordinates to the system with a surfactant droplet under the free water surface. 1, droplet; 2, water surface.

$$\frac{\partial c}{\partial t}+\mathbf{v}\cdot\boldsymbol{\nabla} c=D\Delta c, \tag{3}$$

where the density (ρ), the velocity vector ($\mathbf{v}$), time (t), pressure in the bulk (p), the dynamic viscosity of the liquid (μ), diffusion coefficient (D), and concentration (c) are represented by the variables given.

At the beginning of the dissolution process, the liquid is motionless. In the system, the transfer of the surfactant is due solely to diffusion. When the surfactant reaches the surface (which initially is clean) it is adsorbed primarily in a region close to the droplet. Therefore according to the system geometry, a surfactant concentration gradient and a corresponding gradient in the surface tension result on the surface that produce a convective motion in the liquid. When the viscosity of air is neglected, the following relation gives the viscous stress balance on the free liquid surface

$$\frac{\partial v_t}{\partial z}=-\frac{1}{\mu}\nabla_s\sigma=-\frac{1}{\mu}\frac{d\sigma}{d\Gamma}\nabla_s\Gamma, \tag{4}$$

where v_t is the tangential component of the velocity on the free liquid surface, σ the surface tension, Γ the Gibbs adsorption, z the coordinate normal to the liquid surface (directed downwards, $z=0$ on the free liquid surface), and ∇_s the surface gradient. Here the intrinsic surface viscosity is neglected. Proportionality between the adsorption and bulk concentration [Eq. (5)] as well as between the surface tension and adsorption (Eq. 6) are assumed because the surfactant concentration near the surface is small,

$$\Gamma=\alpha c \tag{5}$$

and

$$\sigma=\sigma_0-RT\Gamma, \tag{6}$$

where α is the Henry constant, R is the gas constant, and T is the temperature.

Assuming the adsorption kinetics are diffusion controlled and mass transfer between the surface and ambient air is absent, Eq. (7) describes how adsorption changes over time,

$$\frac{\partial\Gamma}{\partial t}+\nabla_s(\Gamma v_t-D_s\nabla_s\Gamma)-D\frac{\partial c}{\partial z}=0 \tag{7}$$

where D_s is the surface diffusion coefficient. Here, $\nabla_s(\Gamma v_1)$ describes the contribution of the surface convective flow to the surfactant transfer, $\nabla_s(D_s\nabla_s\Gamma)$, the contribution of the surface diffusion, and $-D\partial c/\partial z$ the contribution of the surfactant exchange between the surface and the bulk solution.

According to the symmetry of the system it is convenient to use the bipolar coordinates η, θ, and φ [20]:

$$\eta=\frac{1}{2}\ln\frac{x^2+y^2+(z+a)^2}{x^2+y^2+(z-a)^2},$$

$$\theta=\frac{i}{2}\ln\frac{(\sqrt{x^2+y^2}-ia)^2+z^2}{(\sqrt{x^2+y^2}+ia)^2+z^2},\quad \tan\varphi=\frac{y}{x}, \tag{8}$$

where a is a constant, and i the imaginary unity. Reverse transformations are

$$x=\frac{a\sin\theta\cos\varphi}{\cosh\eta-\cos\theta},\quad y=\frac{a\sin\theta\sin\varphi}{\cosh\eta-\cos\theta},$$

$$z=\frac{a\sinh\eta}{\cosh\eta-\cos\theta}. \tag{8a}$$

Note that the bipolar coordinate φ coincides with the corresponding cylindrical coordinate. Obviously, according to the system symmetry there is no dependency on this coordinate. For the system under consideration, the bipolar coordinates are presented in Fig. 3 (for simplicity, there the lines for $\varphi=\text{const}$ are absent). Using bipolar coordinates the complicated geometry of the system with a flat interface and a spherical droplet in the bulk is transformed into the simple form of a rectangle bounded by straight lines with $\theta=0$, $\theta=\pi$, $\eta=0$, and $\eta=\eta_0$. Another advantage of the transformation is where the coordinate $\eta\to\infty$. The position is now located within the droplet, and for the calculation we obtain a system of finite dimensions instead of one with infinite dimensions. This simplifies the simulation procedure. The coordinate of the free liquid interface (Cartesian coordinate $z=0$) is $\eta=0$. The interface of the spherical droplet corresponds to a constant coordinate

$$\eta=\eta_0=\operatorname{arccosh}\frac{h}{r_0}=\ln\left(\frac{h}{r_0}+\sqrt{h^2/r_0^2-1}\right)\quad (h>r_0), \tag{9}$$

where r_0 is the droplet radius, h is the distance between the center of the droplet and the free liquid interface. Subsequently the constant a can be found as

$$a=\sqrt{h^2-r_0^2}. \tag{10}$$

It is also convenient to introduce the vorticity ω and the stream function Ψ:

$$\omega=\frac{1}{a}\left(\frac{\partial[(\cosh\eta-\cos\theta)v_\theta]}{\partial\eta}-\frac{\partial[(\cosh\eta-\cos\theta)v_\eta]}{\partial\theta}\right)$$
$$-\frac{2}{a}(\cosh\eta-\cos\theta)\left(\frac{\partial v_\theta}{\partial\eta}-\frac{\partial v_\eta}{\partial\theta}\right),$$

$$v_\eta=\frac{(\cosh\eta-\cos\theta)^2}{a^2\sin\theta}\frac{\partial\Psi}{\partial\theta},\quad v_\theta=-\frac{(\cosh\eta-\cos\theta)^2}{a^2\sin\theta}\frac{\partial\Psi}{\partial\eta}. \tag{11}$$

After introducing the dimensionless variables by means of the equations

$$\tilde{t}=t\frac{D}{a^2},\quad \tilde{\omega}=\omega\frac{a^2}{D},\quad \tilde{\psi}=\psi\frac{1}{aD},\quad \tilde{c}=\frac{c}{c_0}, \tag{12}$$

where c_0 is the surfactant solubility, the set of Eqs. (1)–(3) in the bipolar coordinates takes the form

$$\frac{\partial\tilde{\omega}}{\partial\tilde{t}}+\frac{(\cosh\eta-\cos\theta)^3}{\sin\theta}\left(\frac{\partial\tilde{\psi}}{\partial\theta}\frac{\partial\tilde{\omega}}{\partial\eta}-\frac{\partial\tilde{\psi}}{\partial\eta}\frac{\partial\tilde{\omega}}{\partial\theta}\right)$$

$$-\frac{\tilde{\omega}(\cosh\eta-\cos\theta)^2(1-\cosh\eta\cos\theta)}{\sin^2\theta}\frac{\partial\tilde{\psi}}{\partial\eta}$$

$$+\frac{\tilde{\omega}\sinh\eta(\cosh\eta-\cos\theta)^2}{\sin\theta}\frac{\partial\tilde{\psi}}{\partial\theta}-\mathrm{Pr}(\cosh\eta$$

$$-\cos\theta)^2\left(\frac{\partial^2\tilde{\omega}}{\partial\eta^2}+\frac{\partial^2\tilde{\omega}}{\partial\theta^2}\right)+\mathrm{Pr}\sinh\eta(\cosh\eta-\cos\theta)\frac{\partial\tilde{\omega}}{\partial\eta}$$

$$+\mathrm{Pr}\frac{(\cosh\eta-\cos\theta)(1-\cosh\eta\cos\theta)}{\sin\theta}\frac{\partial\tilde{\omega}}{\partial\theta}$$

$$+\mathrm{Pr}\frac{(\cosh\eta-\cos\theta)^2}{\sin^2\theta}\tilde{\omega}=0, \tag{1a}$$

$$(\cosh\eta-\cos\theta)^3\left(\frac{\partial^2\tilde{\psi}}{\partial\eta^2}+\frac{\partial^2\tilde{\psi}}{\partial\theta^2}\right)+\sinh\eta(\cosh\eta-\cos\theta)^2\frac{\partial\tilde{\psi}}{\partial\eta}$$

$$+\frac{(\cosh\eta-\cos\theta)^2(1-\cosh\eta\cos\theta)}{\sin\theta}\frac{\partial\tilde{\psi}}{\partial\theta}-\tilde{\omega}\sin\theta=0, \tag{2a}$$

$$\frac{\partial\tilde{c}}{\partial\tilde{t}}+\frac{(\cosh\eta-\cos\theta)^3}{\sin\theta}\left(\frac{\partial\tilde{\psi}}{\partial\theta}\frac{\partial\tilde{c}}{\partial\eta}-\frac{\partial\tilde{\psi}}{\partial\eta}\frac{\partial\tilde{c}}{\partial\theta}\right)-(\cosh\eta$$

$$-\cos\theta)^2\left(\frac{\partial^2\tilde{c}}{\partial\eta^2}+\frac{\partial^2\tilde{c}}{\partial\theta^2}\right)+\sinh\eta(\cosh\eta-\cos\theta)\frac{\partial\tilde{c}}{\partial\eta}$$

$$+\frac{(\cosh\eta-\cos\theta)(1-\cosh\eta\cos\theta)}{\sin\theta}\frac{\partial\tilde{c}}{\partial\theta}=0, \tag{3a}$$

where $\mathrm{Pr}=\mu/\rho D$ is the diffusion Prandtl number.

The following initial conditions can be postulated, namely, that the liquid is motionless and the surfactant concentration is equal to its solubility in water at the interface of the surfactant droplet and is zero everywhere else,

$$\tilde{\omega}(\eta,\theta)=0, \quad \tilde{\psi}(\eta,\theta)=0 \quad \text{at} \quad t=0, \tag{13}$$

$$\tilde{c}(\eta,\theta)=\begin{cases}1, & \eta=\eta_0\\ 0, & 0\leqslant\eta<\eta_0\end{cases} \quad \text{at} \quad t=0. \tag{14}$$

According to the system symmetry it holds

$$\tilde{\omega}=0, \quad \frac{\partial\tilde{c}}{\partial\theta}=0 \quad \text{at} \quad \theta=0 \ \text{and} \ \theta=\pi \quad (t>0). \tag{15}$$

Assuming the nondeformable free surface and using the stream line definition we can write

$$\tilde{\psi}=0 \quad \text{at} \quad \theta=0, \ \theta=\pi, \ \eta=0, \ \text{and} \ \eta=\eta_0 \quad (t>0). \tag{16}$$

The boundary condition for $\tilde{\omega}$ at $\eta=\eta_0$ can be obtained from Eq. (2a). Making use of Eq. (16) and the assumption that the droplet surface is motionless, it can be written as

$$\tilde{\omega}=\frac{(\cosh\eta-\cos\theta)^3}{\sin\theta}\frac{\partial^2\tilde{\psi}}{\partial\eta^2} \quad \text{at} \quad \eta=\eta_0 \quad (t>0). \tag{17}$$

It is obvious that

$$\tilde{c}=1 \quad \text{at} \quad \eta=\eta_0 \quad (t>0). \tag{18}$$

Taking into account Eq. (16), the boundary condition (7) at the free liquid surface $\eta=0$ is

$$\frac{\partial\tilde{c}}{\partial\tilde{t}}-\frac{(1-\cos\theta)^3}{\sin\theta}\frac{\partial\tilde{\psi}}{\partial\eta}\frac{\partial\tilde{c}}{\partial\theta}-\frac{D_s}{D}(1-\cos\theta)^2\frac{\partial^2\tilde{c}}{\partial\theta^2}$$

$$-\frac{D_s}{D}\frac{\cos\theta(1-\cos\theta)^2}{\sin\theta}\frac{\partial\tilde{c}}{\partial\theta}-\tilde{c}\frac{(1-\cos\theta)^3}{\sin\theta}\frac{\partial^2\tilde{\psi}}{\partial\eta\partial\theta}$$

$$-\tilde{c}(1-\cos\theta)^2\frac{\partial\tilde{\psi}}{\partial\eta}-\frac{a}{\alpha}(1-\cos\theta)\frac{\partial\tilde{c}}{\partial\eta}=0. \tag{7a}$$

Considering Eqs. (2a) and (16) the expression for the boundary condition of Eq. (4) can be rewritten for $\tilde{\omega}$ at the free surface

$$\tilde{\omega}=-M(1-\cos\theta)\frac{\partial\tilde{c}}{\partial\theta} \quad \text{at} \quad \eta=0 \quad (t>0), \tag{4a}$$

where $M=-(d\sigma/d\Gamma)(d\Gamma/dc)(c_0a/\mu D)$ is the Marangoni number.

NUMERICAL PROCEDURE

The numerical simulation of the dynamic behavior of the system under consideration was carried out on a regular grid by using 31×31 mesh points. It is important that the chosen grid is uniform in the bipolar coordinate system but it is nonuniform in the Cartesian coordinate system. The maximum density of the grid lines is in the region between the interface and the surface of the droplet close to the symmetry axis. The advantage of the chosen approach consists in the more exact calculations for the initial stage of the process when the diffusion and velocity fields are located near the droplet with distances that are not large as compared with the distance between the interface and the droplet. However, the accuracy of the calculations decreases for large distances so that the calculations are less precise for the late stage of the instability development when intensive convective motion propagates far away from the droplet.

The method of successive approaches was applied to solve the elliptic equation (2a) for the stream function, and the one-step explicit finite difference computational method was used to solve the parabolic equations (1a) for the vortic-

ity and (3a) for the concentration. The maximum possible time step for explicit computational methods is determined by the condition of the stability in the numerical scheme [21]. In the simulation procedure presented, the time step was changed within the limits of 10^{-3}–10^{-4} s depending on the process velocity in the system. For the same reason only a unilateral difference of first order (difference ''against the stream'') can be used.

The representation of some of the boundary conditions should be discussed in more detail. The boundary condition for the vorticity at the droplet surface [Eq. (17)] can be evaluated in a number of ways (see, for instance, [22]) giving various orders of precision. Unilateral differences having first order precision were used in the convective terms of Eq. (1a). Equation (17) was also represented by an expression of first order:

$$\tilde{\omega}_{\eta_0,\theta_j}=\frac{(\cosh\eta_0-\cos\theta_j)^3}{\sin\theta_j}\frac{2\tilde{\Psi}_{\eta_0-\Delta\eta,\theta_j}}{(\Delta\eta)^2}. \tag{19}$$

Solving the equation for the stream function [Eq. (1a)] the iteration procedure converges more rapidly when Eq. (19) is used rather than using an expression of second order.

For the boundary conditions of the concentration [Eq. (15)] a better convergence is obtained by the representation of the second order scheme

$$\tilde{c}_{i,0}=\frac{4\tilde{c}_{i,\Delta\theta}-\tilde{c}_{i,2\Delta\theta}}{3}. \tag{20}$$

In order to advance the dependent variables by one time step, the following computational procedures must be carried out: (i) solution of Eqs. (1a) and (3a) for vorticity and concentration at the inner grid nodes using the stream function values of the preceding time step; (ii) solution of Eq. (2a) for the stream function at the inner grid nodes using the vorticity values obtained at the present time step and taking into account the zero values for the stream function at the boundaries; (iii) calculation of the concentration and vorticity values at $\theta=0$, $\theta=\pi$, and $\eta=\eta_0$ from the boundary conditions of Eqs. (15), (17), and (18) taking into account Eqs. (19), (20); (iv) solution of Eq. (7a) for the concentration at $\eta=0$; and (v) calculation of the vorticity values at $\eta=0$ from Eq. (4a) taking into account Eqs. (5) and (6).

In the present paper the simulation results of the following set of the system parameters is considered: the solubility of the surfactant in water $c_0=6.7\times10^{-6}$ mol/cm^3, the Henry constant $\alpha=6.9\times10^{-4}$, the diffusion coefficients in the volume D and in the surface D_s—5×10^{-6} cm^2/s, droplet radius $r_0=1$ mm, and the droplet immersion depth $h=1$ cm. According to [18] the values of the solubility and the Henry constant correspond to the properties of diethyl phthalate. The chosen value of the diffusion coefficient in the volume is close to that estimated by the Wilke-Chang correlation [23] for diethyl phthalate at room temperature. The effect of the surfactant properties on the system behavior will be considered in a forthcoming paper.

RESULTS AND DISCUSSION

The proposed simulation procedure allows us to obtain the values for concentration, stream function, and vorticity at the grid nodes as functions of time and consequently to calculate the distributions of surface velocity, adsorption, and surface tension. This is the basis used to describe the evolution of the system due to the dissolution of the surfactant in the vicinity of the free liquid surface and explain the mechanism of the surface tension auto-oscillations.

The numerical simulation confirms that the main peculiarity of this mechanism arises from a competition between diffusion and convection. The transition of the system in an unstable state is accompanied by a sharp increase of the convection velocity and a simultaneous decrease of the surface tension. Accordingly the system evolution can be divided into two stages, a slow diffusion stage and a fast convective stage.

In the beginning of the slow diffusion stage, the liquid is

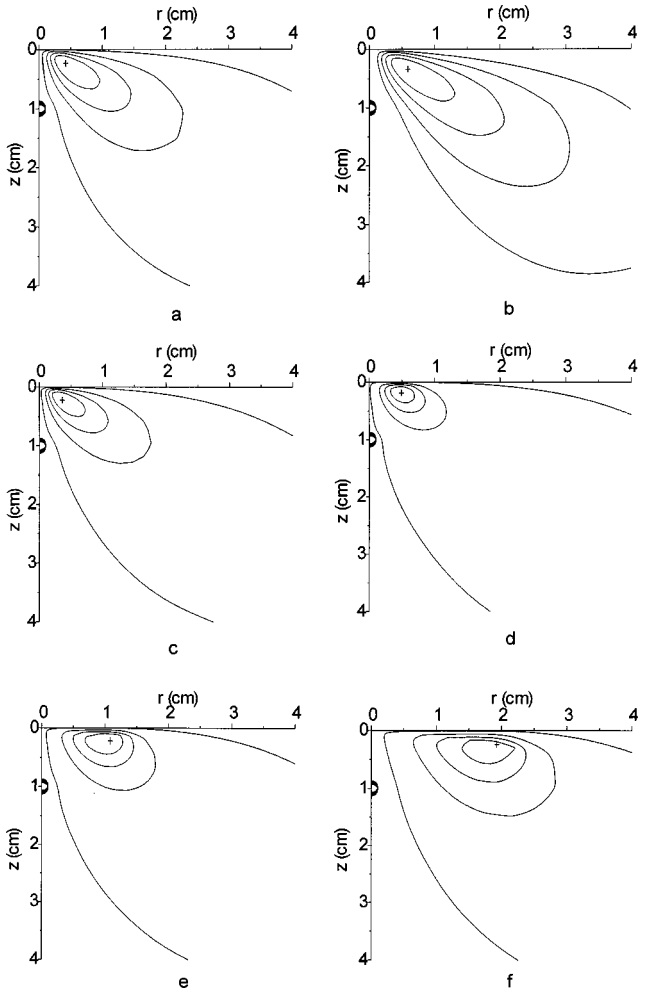

FIG. 4. Convective stream lines in the bulk (a) $t=16$ min after onset of the process, $\tilde{\Psi}_{\max}=3.407\times10^{-8}$, $\Delta\tilde{\Psi}=8\times10^{-9}$; (b) 39 min, $\tilde{\Psi}_{\max}=0.206$, $\Delta\tilde{\Psi}=0.04$; (c) 45 min, $\tilde{\Psi}_{\max}=21.04$, $\Delta\tilde{\Psi}=5$; (d) 45 min 16 s, $\tilde{\Psi}_{\max}=828$, $\Delta\tilde{\Psi}=205$; (c) 45 min 20 s, $\tilde{\Psi}_{\max}=9602$, $\Delta\tilde{\Psi}=2350$; (f) 45 min 22 s, $\tilde{\Psi}_{\max}=45\,923$, $\Delta\tilde{\Psi}=11\,000$.

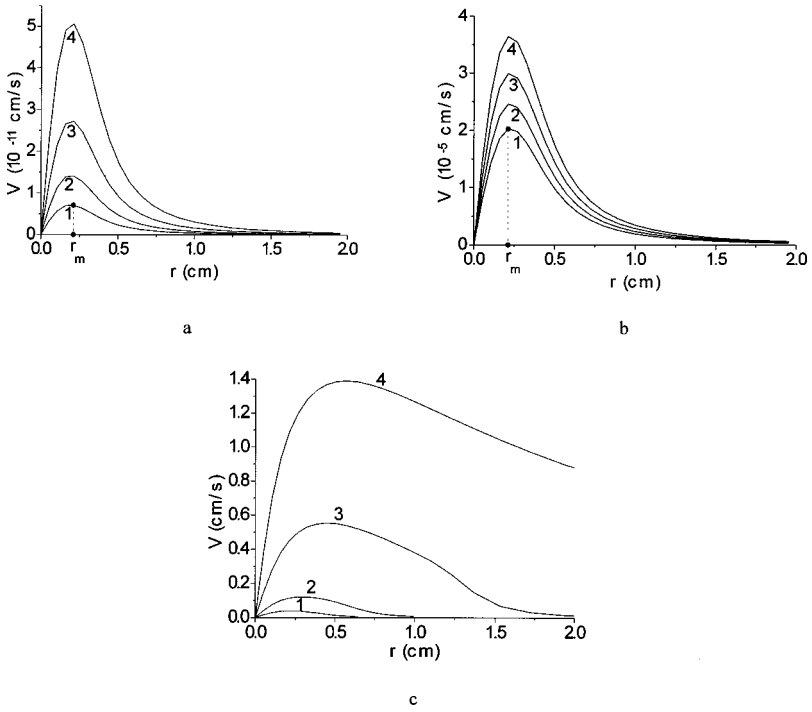

FIG. 5. Surface velocity distribution (a) 1, $t=16$ min after onset of the process 2, $t=16.5$ min; 3, $t=17$ min; 4, $t=17.5$ min; (b) 1, $t=38$ min; 2, $t=38.5$ min; 3, $t=39$ min; 4, $t=39.5$ min; (c) 1, $t=45$ min 12 s, 2, $t=45$ min 16 s, 3, $t=45$ min 20 s 4, $t=45$ min 24 s.

motionless and only diffusion takes place in the system. Over time, in a region close to the symmetry axis, there is an accumulation of surfactant. It has a nonuniform distribution at the surface, and the corresponding surface tension gradient leads to the development of the convective surface motion. During this stage the surface concentration gradient increases slowly and the flow velocity of the liquid remains very small. Therefore the nonlinear convective terms in the Eqs. (3) and (7) are very small, and convection has almost no effect on the concentration field formed due to diffusion of the surfactant. This stage corresponds to the induction period observed in experiments.

In the beginning the stream function has a maximum point situated close to the surface near the symmetry axis. As the convection develops in the bulk, the maximum point is displaced away from its starting location [Figs. 4(a) and 4(b)]. On the other hand, the maximum of the surface velocity moves only at the onset of the process and then remains nearly fixed over a long period of time [Figs. 5(a) and 5(b)]. Even 44 min after the droplet dissolution has begun, the concentration distribution profiles in the bulk have a spherical shape [Fig. 6(a)]. This is an indication that during this time convective motion is still rather weak.

Adsorption causes the accumulation of the solute on the surface, near the axis, as well as an increase in the surface concentration gradient [Fig. 7(a)]. Nevertheless, the increase in surface concentration is still too small to lead to an appreciable reduction in surface tension during the induction period even in the surroundings of the axis.

However, the system becomes unstable after a sufficient amount of surfactant dissolves in the bulk and is adsorbed on the surface. This is characterized by a rapid increase in flow velocity and convective transfer of the surfactant in the system.

According to the equation of the mass conservation in the bulk [Eq. (3)] the change of the solute concentration at any point in the bulk is determined by the balance of diffusion and convective transfer at that point. A comparison of the contributions from convection and diffusion to the change in bulk concentration shows that at approximately 41 min, the contribution of the convective flux becomes larger than the diffusion (initially only in the small region near the symmetry axis at the depth of about 0.15 cm). The increase in the convective region over time is more prominent in the vertical direction, where at 44 min it extends to a vertical depth of 0.9 cm, compared to a maximum of only 0.3 cm in the radial direction. The appearance of a region where convective mass transfer predominates leads to increases in (1) solvent supply to the surface, (2) the surface gradient, and (3) to more intense surface movement. A further increase in velocity intensifies the convective mass transfer producing finally instability in the system.

The surface mass balance equation [Eq. (7)] shows that the surface convection, surface diffusion, and normal diffusion flux from the bulk are responsible for surface concentration changes over time. Let us consider surface region

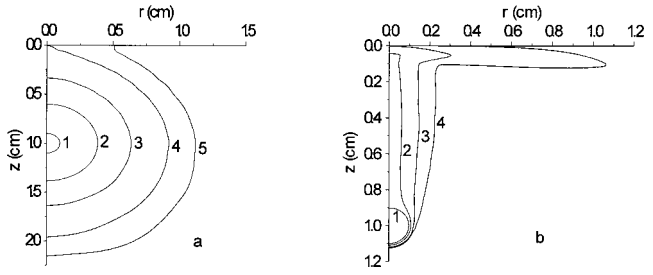

FIG. 6. Concentration distribution (a) $t=44$ min after onset of the process 1, surfactant droplet ($\tilde{c}=1$); 2, $\tilde{c}=2\times10^{-2}$; 3, $\tilde{c}=2\times10^{-4}$; 4, $\tilde{c}=2\times10^{-6}$; 5, $\tilde{c}=2\times10^{-9}$. (b) $t=45.5$ min, 1, the surfactant droplet ($\tilde{c}=1$); 2, $\tilde{c}=0.3$; 3, $\tilde{c}=0.03$; 4, $\tilde{c}=0.003$.

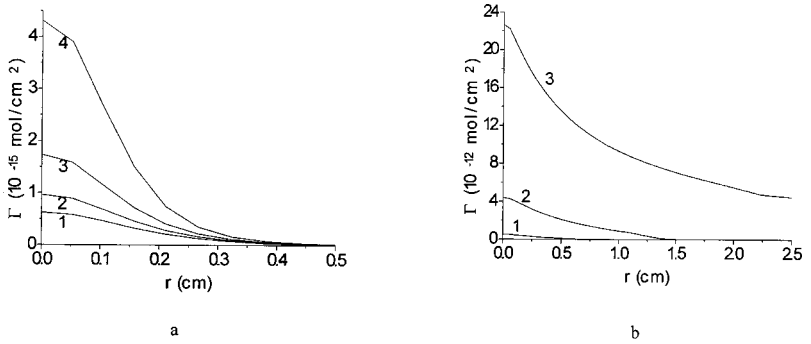

FIG. 7. Adsorption distribution: (a) 1, $t=43$ min after onset of the process; 2, $t=43.5$ min; 3, $t=44$ min; 4, $t=44.5$ min (b) 1, $t=45$ min 16 s; 2, $t=45$ min 20 s; 3, $t=45$ min 24 s.

near the axis. Here diffusion from the bulk supplies the solvent to the surface producing a positive change in surface concentration. While surface convection and diffusion reduce the surface concentration by moving surfactant away from the axis. When a predominant region of convective mass transfer appears in the bulk, fluxes show a rapid increase, but the normal diffusion transfer exceeds surface convection and surface concentration increases near the symmetry axis. The intense convective motion near the symmetry axis causes the displacement in the stream function's maximum point back to the axis [Fig. 5(c)]. It should be noted that the surface diffusion flux is always some orders of magnitude lower than both the surface convection and normal diffusion, therefore its effects are negligible.

The situation in the distant regions is more complicated. The normalized contribution of the different mechanisms to mass transfer on the surface for $r=0.21$ cm (the point where the surface velocity is maximal during the slow stage) is presented in Fig. 8. In the beginning the contributions from

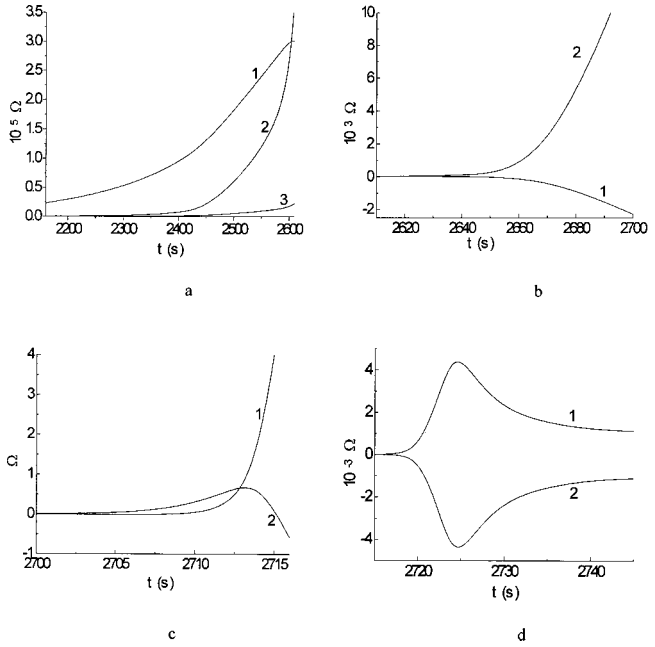

FIG. 8. Mass transfer at the surface at $r=0.21$ cm. 1, contribution of the normal diffusion flux $[\Omega_n=-(a^2/\alpha DC_0)D\partial c/\partial z]$; 2, contribution of the convective flux $[\Omega_c=(a^2/\alpha DC_0)\nabla_s(\Gamma v_t)]$; 3, contribution of the surface diffusion flux $[\Omega_D=(a^2/\alpha DC_0)\nabla_s(D_g\nabla_s\Gamma)]$.

all of the above mentioned fluxes produce positive changes in the surface concentration. The normal diffusion from the bulk provides the main contribution. Originally the contribution from the convective surface flux is very small, but after 43 min it is of the same order as the contribution from the normal diffusion flux [Fig. 8(a)]. The contribution from the surface diffusion is always rather small so that it is not presented in Figs. 8(b), 8(c) and 8(f).

The instability develops in the vicinity of the symmetry axis where the largest concentration gradient occurs. Initially the convective flux brings surfactant solution with a higher concentration to the surface so that the growing instability is sustained. The surfactant is rapidly transferred from the axis to remote parts of the surface by convection. This results in the development of an opposing concentration gradient between the surface and the bulk leading to a partial desorption of the surfactant [i.e., a negative flux, Fig. 8(b)] as the concentration in the bulk phase near the surface increases slowly. It should be emphasized that the opposite concentration gradient near the surface is localized to a particular region. Over time, this region displaces away from the symmetry axis. Nevertheless the surface concentration continues to grow as the positive contribution from the surface convective flux outweighs the negative contribution of the normal diffusion flux.

As the surfactant spreads, more distant regions of the surface are involved in the motion [Fig. 5(c)]. Consequently, convection develops in the bulk [Figs. 4(d), 4(e), and 4(f)] accelerating the transfer of surfactant even to remote regions of the surface. Over time, this transfer leads to an increase in both bulk concentration near the surface, and once again a positive normal diffusion flux towards the surface [Figs. 8(c) and 8(d)].

The fast spreading of the surfactant over the surface [Figs. 6(b) and 7(b)] corresponds to a very fast ($\leqslant$10 s) decrease in surface tension (Fig. 9). Simultaneously, the surface velocity increases (Fig. 10) and the maximum point of the stream function moves away from the axis [Figs. 4(d), 4(e), and 4(f)].

The surface velocity is not uniform. It is zero at the symmetry axis, increases with the distance to a maximum, and then decreases (Fig. 5). Surface dilatation is observed in regions where the velocity increases, whereas surface compression occurs where the velocity decreases. Likewise, near the axis, a fast increase in the surface velocity with time pro-

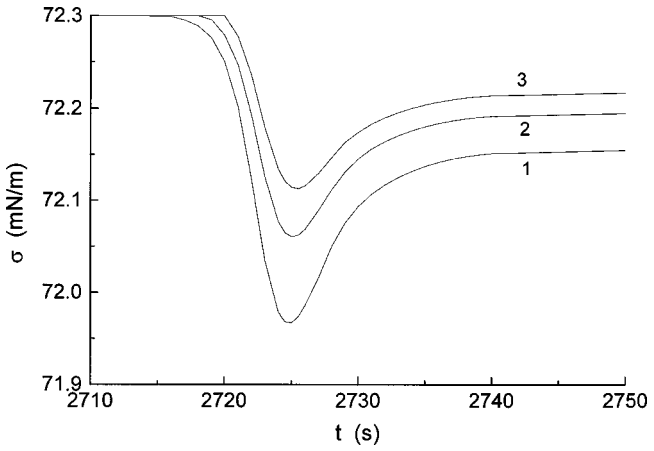

FIG. 9. Surface tension vs time after onset of the instability at different distances from the symmetry axis: 1, 5 mm; 2, 10 mm; 3, 15 mm.

duces a fast dilatation of the surface. The convective surface flux contribution becomes negative [Fig. 8(c)] and increases rapidly with time in the absolute value [Fig. 8(d)]. The surface concentration increases and the surface tension decreases until the contribution of the normal diffusion flux exceeds that of the negative convective surface flux. At approximately 45 min 25 s both contributions compensate each other. The surface concentration approaches a maximum, and correspondingly the surface tension exhibits minimum (Fig. 9). Then the surface expansion begins to prevail, the surface concentration decreases and the surface tension increases. Simultaneously both the surface convective flux and the normal diffusion flux decrease in the absolute value [Fig. 8(d)].

Convection spreads the surfactant over the surface and distributes it in the bulk mixing it with the more dilute solution. The mixing of the surfactant reduces the concentration gradients in the system. As a consequence of the more uniform distribution of surfactant the system is returned to the stable state and the surface velocity gradually decreases (Fig. 10).

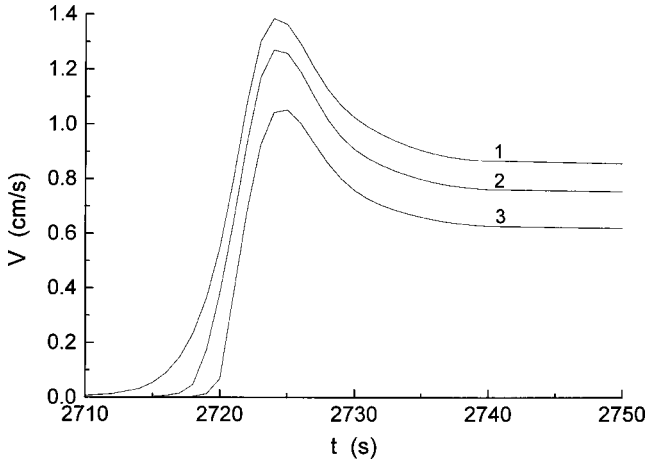

FIG. 10. Velocity at the free water surface vs time after onset of the instability at different distances from symmetry axis: 1, 5 mm; 2, 10 mm; 3, 15 mm.

It is seen from Fig. 9 that the maximum decrease in the surface tension (oscillation amplitude) depends on the distance from the symmetry axis. This result corresponds to the experimental data recently obtained. It was revealed by the experiments with a diethyl phthalate droplet that the oscillation amplitude decreases from 2–2.5 mN/m to approximately 1.5 mN/m by increasing the distance between the capillary and the Wilhelmy plate from 15 to 30 mm [19].

The analysis shows that the performed numerical simulation reflects the main peculiarities of the surface tension auto-oscillations experimentally observed. However, there are some distinctions connected with the chosen model. The theoretical model considers a semi-infinite liquid layer, whereas the real experimental systems are bounded. Furthermore, a system without a capillary was theoretically considered. In reality it takes some limited (rather short) time to spread surfactant over the whole surface and the convective motion damps faster owing to viscous dissipation on the capillary and the vessel walls. The oscillation amplitude is expected to be larger and the duration of the induction period expected to be shorter in real systems because of their limited dimensions.

The numerical model has also a limitation connected with the large grid step in the distinct regions of the system. It follows from the calculations that in the late stage of the process development, the intensive convective motion propagates with distances much larger than those between the interface and the droplet. As discussed above, the precision of the calculations drops in this case, so that the results become less reliable. Thus, the calculations cannot be continued till the complete convection damping that is just the precondition for the next oscillation. Therefore only the first oscillation can be considered in the frameworks of the chosen numerical model but not the periodicity.

Nevertheless the chosen model permits a good description of the system dynamics in the initial period, because the processes in the distant parts of the system do not influence its behavior during the whole induction period. The calculations give reliable values of the induction period comparable with the experimental data. The general shape of the oscillation can be simulated. The calculations are able to predict both the abrupt decrease in the surface tension at the beginning of the instability followed by the surface tension minimum and the following increase due to surface dilatation near the axis and partial surfactant desorption in the distant regions. Although the numerical model allows to consider only the first oscillation, it shows an obvious tendency for the system to revert to the initial stable state, which is a precondition for the next oscillation.

The concrete comparison with experimental results will be a subject of further considerations. Particularly the effect of the surfactant properties such as solubility, surface activity, and bulk diffusion coefficient on the system behavior can provide additional information. During the induction period the main processes are located near the symmetry axis so that the system dimensions seem not be significant for the begin-

ning of the instability. Therefore, the induction times calculated with the numerical model will correspond to those found in the experiments.

CONCLUSIONS

The numerical simulation allows a comprehensive description of the mechanism of surface tension auto-oscillations observed experimentally in a system with a low soluble surfactant droplet placed under the free water surface. A simulation was carried for the case of a semi-infinite liquid volume on the basis of the nonlinear, nonstationary state equations of fluid mechanics taking into account the dynamic adsorption of the surfactant. The numerical solution of the problem allows one to trace a series of consecutive changes in the system during the process of saturation of water by surfactant. The development of instability produced by the Marangoni effect can be considered in this way.

As the chosen model deals with a semi-infinite system, it describes only the initial period of the system evolution and cannot reflect the whole series of the auto-oscillations. Nevertheless the model provides the main features of the process under consideration: the existence of the induction out time when surface tension remains practically constant, the sharp decrease of the surface tension when instability arises, and the gradual increase of the surface tension when the convective motion fades. This points the return of the system to the stable state. The overall process can be subdivided into two stages.

The initial slow stage is characterized mainly by diffusion transfer of the surfactant from the droplet into the liquid. The surface adsorption gradient and consequently, surface tension gradient gradually increase over time. At first the system shows a small convection velocity that does not contribute appreciably to the transfer of surfactant. The increasing adsorption gradient on the surface is the driving force responsible for increasing velocities, both surface and bulk, and also the normal concentration gradient near the surface. The maximum of the adsorption and normal concentration gradients located near the symmetry axis causes the development of instability in this particular region after a sufficient amount of surfactant accumulates there.

The second (fast) stage starts when the system becomes unstable. At this point all parameters of the system show a rapid change. The instability begins to develop when the convective transfer becomes dominating in a small region in the bulk around the symmetry axis. The growing instability is sustained by a normal concentration gradient. The numerical results allow a comparison of diffusion and convective solute transfer, both in the bulk and on the surface, during the different stages of the process. Initially the convective surface flux brings the surfactant from the axis to the remote parts of the surface and increases surface adsorption, but later it tends to reduce the adsorption producing a fast surface expansion. The adsorption increases as long as the normal diffusion flux prevails on the effect of surface dilatation that is accompanied by a decrease in surface tension. After the surface dilatation becomes predominant the surface tension commences to increase. A strong convective flux spreads the surfactant over the surface and mixes the bulk solution. After a more dilute solution is supplied to the surface the concentration gradients decrease and the system returns to the stable state.

The numerical results confirm the mechanism of the surface tension auto-oscillations described qualitatively in a recent paper [18] and allow the understanding of the main regularities of the system behavior experimentally observed.

ACKNOWLEDGMENTS

Financial assistance by the Bundesministerium für Bildung, Wissenschaft, Forschung und Technologie (BMBF) (Project No. UKR-014-98) is gratefully acknowledged. N.M.K. thanks the Max-Planck Gesellschaft for the financial support.

[1] *Convective Transport and Instability Phenomena*, edited by J. Zierep and H. Oertel (Braun, Karlsruhe, 1982).
[2] P. Schwartz, J. Bielecki, and H. Linde, Z. Phys. Chem. **266**, 731 (1985).
[3] H. Linde and P. Schwartz, Nova Acta Leopold. **61**, 105 (1989).
[4] D. Schwabe, U. Moller, J. Schneider, and A. Scharmann, Phys. Fluids A **4**, 2368 (1992).
[5] S. Bekki, M. Vignes-Adler, and E. Nakache, J. Colloid Interface Sci. **152**, 314 (1992).
[6] M. Santiago-Rosanne, M. Vignes-Adler, and M. G. Velarde, J. Colloid Interface Sci. **191**, 65 (1997).
[7] E. Tan and S. T. Thoroddsen, Phys. Fluids **10**, 3038 (1998).
[8] A. Wierschem, M. G. Velarde, H. Linde, and W. Waldhelm, J. Colloid Interface Sci. **212**, 365 (1999).
[9] C. V. Sternling and L. E. Scriven, AIChE J. **5**, 514 (1959).
[10] M. Hennenberg, T. S. Sorensen, and A. Sanfeld, J. Chem. Soc., Faraday Trans. 2 **73**, 48 (1977).
[11] T. S. Sorensen, F. Y. Hansen, J. N. Nielsen, and M. Hennenberg, J. Chem. Soc., Faraday Trans. 2 **73**, 1589 (1977).
[12] T. S. Sorensen, M. Hennenberg, and F. Y. Hansen, J. Chem. Soc., Faraday Trans. 2 **74**, 1005 (1978).
[13] T. S. Sorensen, J. Chem. Soc., Faraday Trans. 2 **76**, 1170 (1980).
[14] J. Reichenbach and H. Linde, J. Colloid Interface Sci. **84**, 433 (1981).
[15] X.-L. Chu and M. G. Velarde, J. Colloid Interface Sci. **131**, 471 (1989).
[16] C. F. Chen and T. F. Su, Phys. Fluids A **4**, 2360 (1992).
[17] J. Bragard, S. G. Slavtchev, and G. Lebon, J. Colloid Interface Sci. **168**, 402 (1994).
[18] V. I. Kovalchuk, H. Kamusewitz, D. Vollhardt, and N. M. Kovalchuk, Phys. Rev. E **60**, 2029 (1999).

[19] N. Kovalchuk and D. Vollhardt, J. Phys. Chem. **104**, 7987 (2000).
[20] N. N. Lebedev, *Special Functions and Their Applications* (Dover, New York, 1972).
[21] P. J. Roache, *Computational Fluid Dynamics* (Hermosa, Albuquerque, NM, 1976).
[22] W. R. Briley, J. Fluid Mech. **47**, 713 (1971).
[23] R. C. Reid, J. M. Prausnitz, and T. K. Sherwood, *The Properties of Gases and Liquids* (McGraw-Hill, New York, 1977).